

Langmuir Probe Measurements of Spatial Plasma Profiles and Temporal Dependences in a DC-Energized Hollow-Cathode Plasma Jet System

Milan Tichý¹, Zdeněk Hubička², Petr Virostko², Irena Picková¹, Miloš Šícha^{1,2}, Martin Čada², Jiří Olejníček², Olexandr Churpita², Lubomír Jastrabík², Petr Adámek², Pavel Kudrna^{1,2}, Jan Klusůň^{1,2}, Sergey Leshkov¹, Mariya Chichina², Štěpán Kment²

¹ Charles University in Prague, Faculty of Mathematics and Physics, Department of Surface and Plasma Science, V Holešovičkách 2, 180 00 Prague 8, Czech Republic

² Institute of Physics, Academy of Sciences of the Czech Republic, v.v.i., Na Slovance 2, 182 21 Prague 8, Czech Republic

(Received: 1 September 2008 / Accepted: 21 February 2009)

We present results of the Langmuir probe diagnostics of the hollow-cathode plasma jet system. The spatial distribution of the plasma parameters in the DC plasma jet discharge was studied as well as their temporal dependence in case when the system was operated in a pulsed DC regime. The pulsed DC discharge was ignited with a continuous RF discharge of a small power on the background to allow repetitive ignition of the DC hollow-cathode discharge.

Keywords: Langmuir probe, plasma jet system, spatial distribution, pulsed discharge

1. Introduction

Plasma jet systems generated by low-pressure hollow cathode discharges were developed some two decades ago [1]. Hollow cathode discharges are excited by RF, or DC continuous, or pulsed voltage [2,3,4]. The hollow cathode acts also as a nozzle for the working gas flow. Systems with a hollow cathode require as a rule a relatively low gas pressure of the order of several Pa up to several hundred Pa. The advantage of plasma jet systems is that they are able to deposit thin films inside cavities and holes and on substrates with complex substrate shapes at a comparatively high deposition rate.

Low-pressure plasma-chemical systems with plasma jets have been widely used for thin films deposition of different materials, e.g. TiN [5], AlN [6], CrN [7], Cu₃N [8], TiO_x [9], Al₂O₃ [6], CN_x [10], diamond-like-carbon (DLC) layers [11] and LiCoO_x [12]. In these applications, usually a metallic or single component hollow cathode was reactively sputtered in a suitable working gas. The papers [13,14] present deposition of the Ba_xSr_{1-x}TiO₃ films by means of single plasma jet system and paper [15] the application of a double hollow cathode system in which separate two hollow cathodes were made of BaTiO₃ and SrTiO₃ ceramics. During the deposition both hollow cathodes were reactively sputtered in a mixture of Ar and O₂. The experimental set up allowed one to change the stoichiometric composition of the film during the experiment and hence to deposit layers with a compositional gradient of Ba and Sr materials along the thickness of the film.

In the last couple of decades the two collaborating groups of authors of this contribution have been

investigating the low-pressure hollow-cathode plasma jet with the intention of applying it for deposition of thin films of interesting materials and with the intention to gain a better understanding of the processes occurring in these systems. When appropriate, pulsed method of operation was applied. As it is well known, pulsed operation brings advantages that can be summarized as follows (see e.g. [16]):

- Control of the heat load onto the substrate.
- Control of the ion/neutral flux to the substrate.
- Limitation of the substrate ion bombardment; reduction of the compressive stress in the film.
- Control of the dissociation of the precursor; reduction of the precursor fragmentation.

It is clear that the reproducibility of the deposited thin films requires ensuring constancy of the plasma properties in every repetition of the thin film deposition process. During the deposition process it is advisable to use such plasma diagnostic methods that are able to determine the plasma parameters using as simple a diagnostic procedure as possible. In this article we shall concentrate on the determination of plasma parameters in the low-pressure hollow-cathode plasma jet system using as a diagnostic tool the Langmuir probe technique.

2. The Langmuir probe diagnostic technique

Measurements with electric probes belong to the oldest as well as to the most often used procedures for diagnosing low-temperature plasma. The method was developed by Langmuir and his co-workers in 1920s [17]. Since then it has been subject to many extensions and

further developments in order to extend its applicability to more general conditions in comparison to the ones investigated by Langmuir. Such investigations proceeded continuously and the research on extension of applicability of Langmuir probe diagnostics continues also in the present time. There are several books devoted to probe diagnostic, e.g. [18,19] as well as interesting review papers, e.g. [20,21]. A recent review of the features of the Langmuir probe method can be found in [22]. Therefore a brief description will be given here.

The spatial resolution of the probe method is given by the probe dimensions or it is of the order of magnitude of the Debye length $\lambda_D = \sqrt{\frac{\epsilon_0 k_B T_e}{q_0^2 n_e}}$, whatever is greater. In

case of our spatially resolved measurements in a CW DC discharge the probe radius $r_p = 22.5 \mu\text{m}$. The Debye length $\lambda_D \approx 5\text{--}52 \mu\text{m}$ ($T_e \approx 0.5\text{eV}$, $n_e \approx 10^{16}\text{--}10^{18}\text{m}^{-3}$). Hence the spatial resolution of the probe is approximately given in our conditions by the probe diameter $\sim 50 \mu\text{m}$. In the pulsed case ($r_p = 190 \mu\text{m}$, $T_e \approx 1.5\text{eV}$, $n_e \approx 8 \times 10^{16}\text{m}^{-3}$, $\lambda_D \approx 32 \mu\text{m}$) the spatial resolution is also given by the probe diameter; this time equal to $\sim 380 \mu\text{m}$.

The temporal resolution of the probe itself is approximately given by the time of travel of ion across the sheath. Since the ions at the sheath boundary are accelerated in the pre-sheath approximately up to the electron temperature and the sheath thickness is of the

order of λ_D , we obtain for the time resolution τ_r the expression $\tau_r \sim \sqrt{\frac{\epsilon_0 m_i}{q_0^2 n_i}}$; here m_i , n_i denote the mass and density of a positive ion. For our experimental conditions, Ar ions and plasma density 10^{17}m^{-3} we obtain the time resolution $\tau_r \approx 0.3 \mu\text{s}$.

There are not many procedures that permit the direct experimental determination of the electron energy distribution function (EEDF) in a plasma; one of them is based on probe measurements (in collision-less regime). The Druyvesteyn relation [23] states that

$$\frac{d^2 I_{pe}}{du_p^2} = \frac{q_0^{\frac{3}{2}}}{2^{\frac{3}{2}}} m_e^{-\frac{1}{2}} n_e A_p \bar{f}(u_p),$$

where the electron energy distribution function $\bar{f}(u_p)$ fulfils the normalizing condition

$$\int_0^\infty \bar{f}(u_p) u_p^{\frac{1}{2}} du_p = 1.$$

The symbols I_{pe} , u_p , q_0 , m_e , n_e , A_p represent the electron part of the probe current, retarding probe voltage with respect to space potential, elementary charge, electron mass, electron density and probe collecting area respectively. Applicability of this method is limited to conditions where the length of electron energy relaxation

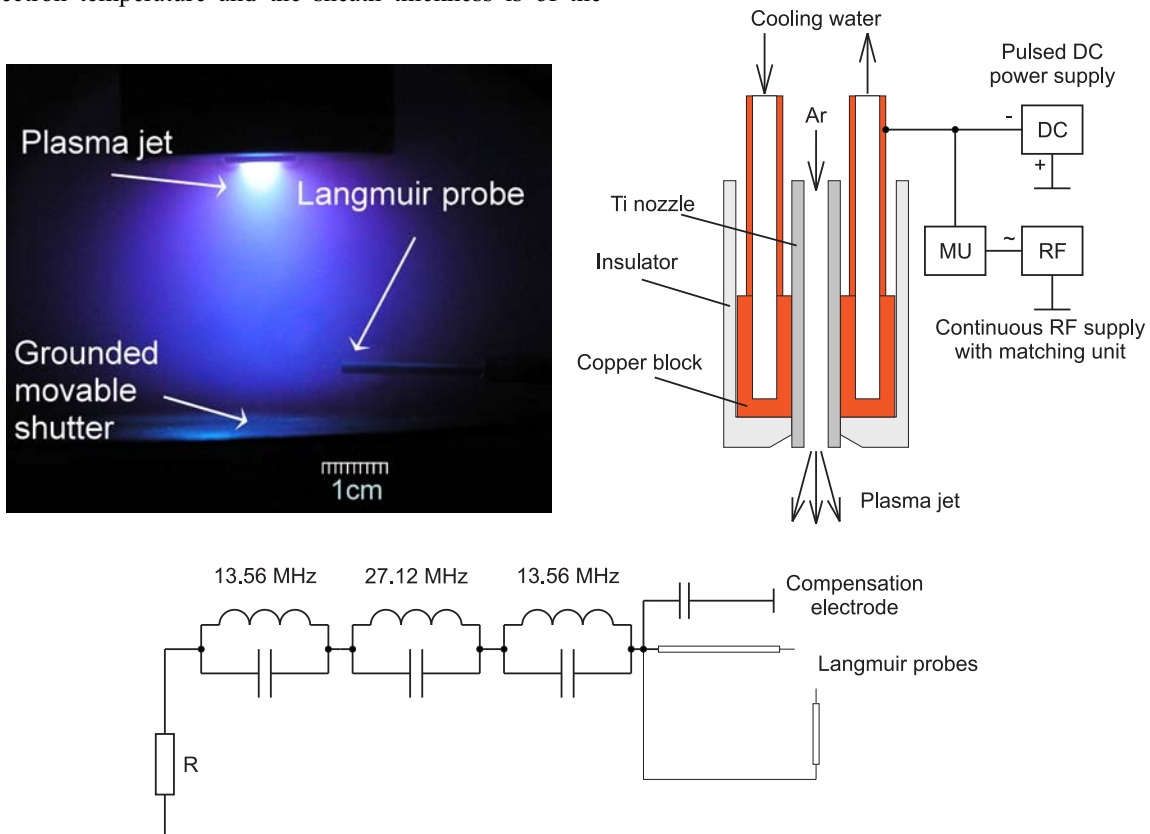


Fig. 1. The schematic diagram of the low-pressure plasma jet system. Only the plasma nozzle located at the axis of the grounded cylindrical vacuum vessel with the diameter of 300 mm is shown. In the top left corner a photo of a typical discharge is introduced. The details on the system and experimental conditions are given in the text.

in both electron-electron and electron-neutral collisions is much bigger than dimensions of the probe and of the near-probe perturbation region.

3. Langmuir probe measurements in the low-pressure plasma jet system - results and discussion

The experimental set up of our plasma jet system is shown in Fig. 1. Since the significant part of the generator power is dissipated on the hollow cathode, the nozzle has to be water-cooled. It was mounted coaxially inside of the earthed cylindrical stainless-steel UHV chamber with the diameter of 300 mm. The system allowed generation of the hollow cathode discharge by four different means: by DC or RF power in CW or pulsed operation; we report here the CW DC mode and the pulsed DC mode of operation. However, when using pulsed DC power the low CW RF power of about 30 W had to be used in parallel with a DC pulsed source, see Fig. 1. This configuration allowed the DC hollow cathode discharge to start easily in each period. The nozzle in our experiments was made of titanium. Approximately 50 mm downstream of the nozzle a grounded shutter was located that could be moved out of the system axis by means of a rotary feed-through. The reported plasma parameters, however, did not depend significantly on the shutter position. The substrate table (not shown in Fig. 1) was positioned approximately 1 cm below the shutter. The shutter was used during the initial phase of layer deposition to protect the substrate before the plasma parameters reached the required values. In case that the deposition rate was high the shutter also enabled to precisely determine the deposition time.

In order to minimize the effect of the RF power source to the probe measurements we applied the “combined” probe compensation method which uses filters as well as an auxiliary electrode coupled to the probe prior to the filters as described in [24], see Fig. 1. The radius r_p of the used cylindrical tungsten probe was

190 μm and its length 2.5 mm. This comparatively bulky probe is better suited for measurements in an RF plasma when there are not strict requirements for space resolution of the method. The reason is that the disturbing RF voltage is proportional to the sheath impedance that decreases with increasing probe size [25]. For measurements in a CW DC discharge a thinner probe ($r_p=22.5 \mu\text{m}$, $l_p=3 \text{ mm}$) was used and the probe compensation was not applied. For the probe measurements the grounded vacuum vessel served as a reference electrode. During measurements in CW DC discharge the probe was radially movable, however for time-resolved measurements in pulsed mode of operation the probe was placed at the jet axis. The distance of the probe downstream of the nozzle exit (in figures denoted as h) was adjustable by shifting the whole nozzle system up and down using a bellows-sealed linear motion feedthrough constructed especially for this purpose. The applied time-resolved technique allowed measurements of the probe characteristic with a time resolution of about 10 μs . The pressure of the working gas inside the reactor vessel was low enough so that the influence of collisions of charged particles in the space charge sheath on the probe characteristic could be neglected. The applied method of plasma parameter determination from the probe data was thus the standard one. In cases when the measured EEDF was not close to Maxwellian the electron density n_e and the mean electron energy E_{mean} were determined from the integrals of the measured EEDF.

It is to be noted, however, that the pressure inside the (cylindrical) nozzle does not correspond to the pressure in the reactor chamber. From thermodynamic considerations one can show that the pressure p_N at the nozzle outlet is proportional to the mass flow rate of the working gas Q and to the square root of the nozzle temperature T_N : $p_N \sim QT_N^{1/2}$. While in the cylindrical nozzle the gas speed cannot exceed the sonic value, after expansion into the reactor vessel the gas flow can exceed

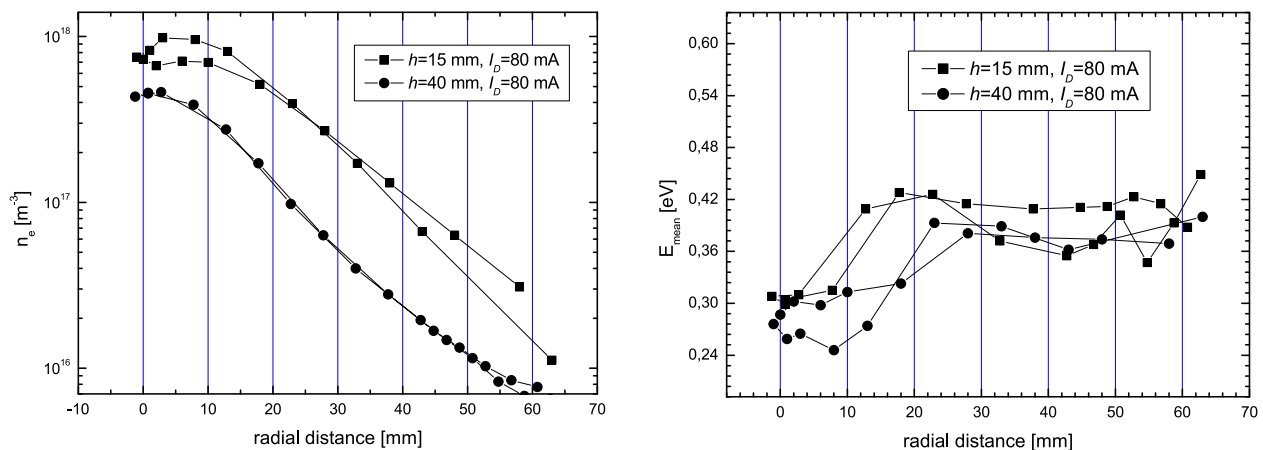


Fig. 2. The radial dependences of electron density (left panel) and of electron mean energy (right panel) in the DC-powered single plasma jet system. Ti nozzle diameter 6 mm, pressure 20 Pa, argon flow 30 sccm.

the speed of sound.

In Fig. 2 we give the results of spatially-resolved probe measurements in the DC plasma jet in argon in continuous regime. The diameter of the Ti nozzle was 6 mm, chamber pressure 20 Pa, argon mass flow rate 30 sccm, other experimental conditions are indicated in the figure. Measurements were performed at two different distances of the probe downstream of the nozzle end: $h=15$ mm and $h=40$ mm. We see three interesting features: (i) the maximum of the electron density does not correspond to the system axis; (ii) mean electron energy is higher in the periphery of the plasma jet than at its axis and (iii) the electron density decays rather slowly towards the vessel walls. Feature (i) we attribute to the fact that inside the hollow cathode most of the charged particles are created close to the hollow cathode inner surface [26], feature (ii) probably links to the formation of the plasma jet by the gas flow as explained below in discussion of the results gained in pulsed mode of operation. Feature (iii) is probably coupled with the fact that the discharge current is distributed across a large area of the anode - the grounded vessel - and the radial electric field is almost zero up to approximately 3 cm from the axis and then even weakly retarding (a few tenths of volts per cm). From the data, the reproducibility of the experiment may be assessed: the radial dependences were measured by changing the radial probe position in the direction towards the axis at certain probe positions and in the opposite direction at positions intermediate to the former ones. The quality of the data enabled us also to estimate the EEDF by the Druyvesteyn method described above. At 20 Pa the collision-less conditions for the validity of Druyvesteyn relation are namely fulfilled. The EEDF featured the for argon characteristic “double temperature” shape up to the radii around 10 mm from the system axis, further from the axis (for radii greater than approximately 20 mm) the EEDF was Maxwellian.

The evaluation of the electron mean energy from the integral of the EEDF (instead of estimating the “electron temperature” from the slope of the probe characteristic) was therefore well substantiated.

Time-resolved Langmuir probe measurements of plasma parameters in a periodically pulsed DC plasma jet discharge in argon are depicted in Fig. 3. The discharge current during the active impulse was 5 amps, other experimental conditions are given in the figure caption. The probe was positioned at the nozzle axis. In order to be able to reliably switch-on the discharge the “starting” RF power of about 30W was applied continuously. That RF power created “background” plasma in the idle part of the period due to the capacitive asymmetric RF discharge between the RF powered nozzle and the grounded reactor vessel. That was an RF discharge of the so-called α -type; i.e. most of charged particles were created in the plasma volume. The parameters of this “background” plasma for $h=20$ mm were $n_e \approx 10^{16} \text{ m}^{-3}$, $T_e \approx 6\text{-}7$ eV. This comparatively high electron temperature was probably due to the large negative RF bias on the nozzle electrode. This negative DC bias amounted to approximately -80 V at the peak-to-peak RF voltage roughly 330V, see Fig. 4. In this “background” plasma the pulsed DC hollow cathode discharge was ignited inside the nozzle at the beginning of the active part of the period.

In Fig. 3 we see the comparatively sharp edges of the discharge current and the characteristic “double-peak” shape of the temporal dependence of the electron density in the active pulse. Qualitative explanation of this structure is as follows: immediately after application of the voltage the “background” plasma is enhanced while the hollow cathode discharge does not yet burn inside the nozzle. When the hollow cathode discharge starts, matching conditions change and the background RF discharge extinguishes (the RF-formed bias ceases). The intense plasma inside the hollow cathode is then blown

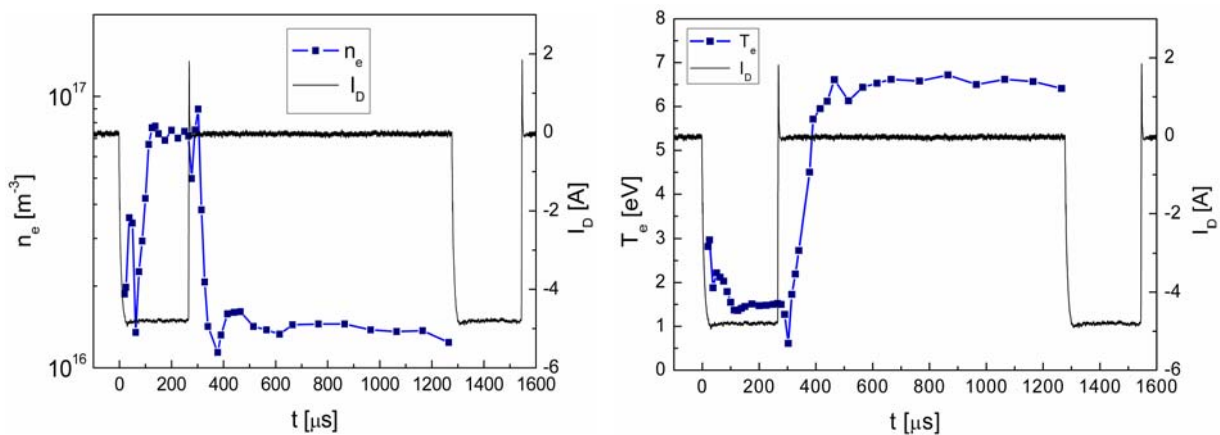


Fig. 3. The temporal dependences of electron density (left panel) and of electron temperature (right panel) in the DC-powered single plasma jet system in pulsed regime in argon. Ti nozzle diameter 6mm, pressure 3.5 Pa, argon flow 110 sccm, $h=20$ mm. Repetition rate 575 Hz, duty cycle 0.175, active pulse length 270 μs . Discharge current during the active part of the period 5 A. The plasma parameters in the idle part of the period correspond to the background RF plasma.

out of the nozzle by the working gas flow. In addition to the γ processes on the hollow cathode surface inside the hollow cathode the ionization proceeds by two further mechanisms: by volume ionization due to “pendulum” electrons that swing from one side of the hollow cathode to the other and gain energy in the cathode fall, and by photo-ionization due to intensive radiation inside the hollow cathode. That qualitatively explains that the “body” of the EEDF contains electrons created in the hollow cathode that have a comparatively low temperature, see Fig. 3. Since the plasma flow expands into the volume with lower pressure its speed is likely to be supersonic (see e.g. [5]) and forms a visible jet below the nozzle. Such an idea is supported by the work [27]. The hydrodynamics of the flow confines the heavy charged particles that in turn reduce the fast radial diffusion of electrons. After switching off the discharge voltage first the hollow cathode discharge extinguishes and that is accompanied by the instantaneous decrease of both the electron density and temperature. Then the RF discharge takes over and creates low density plasma with comparatively high electron temperature.

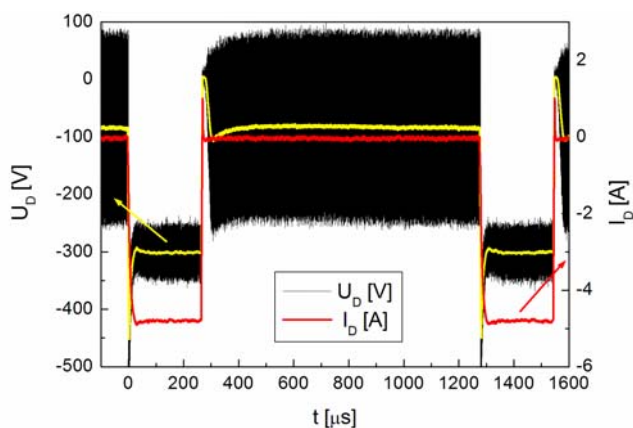


Fig. 4 The temporal dependences of DC discharge voltage and discharge current. The superimposed CW RF voltage is also shown. The experimental conditions are the same as that in Fig. 3.

Fig. 4 indicates the temporal course of the voltage applied on the nozzle with the discharge current that is also indicated in Fig. 3. The time-averaged DC voltage is also shown in yellow color together with the discharge current in red color. We see that the DC voltage on the nozzle electrode does not drop to zero in the pulse idle state but reaches a value around -80 V. That is the negative DC bias due to the applied RF voltage with the peak-to-peak value around 330 V. We also see in Fig. 4 that the amplitude of the applied RF voltage drops down to peak-to-peak value around 100 V during the active phase of the DC pulse. That is due to improper matching of the RF generator (the discharge impedance has changed during the active pulse and there was the output impedance of the DC power supply in parallel to that).

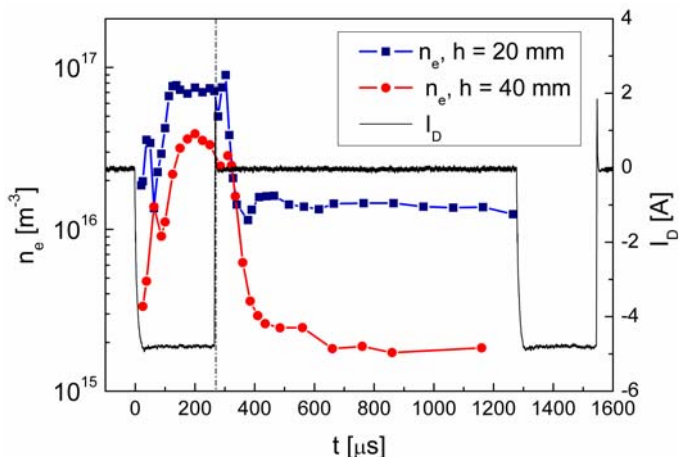


Fig. 5 The temporal dependences of electron density in the DC-powered single plasma jet system in pulsed regime in argon at two different distances from the nozzle exit. The experimental conditions are the same as that in Fig. 3.

Fig. 5 gives information on the spatial variations of the time dependence of the electron density in the pulse mode operation of the plasma jet. The data is taken at the same experimental conditions as that in Fig. 3, but at two different distances from the nozzle output: 20mm and 40mm. It is evident that the characteristic “double peak” structure remains during the active pulse also further from the nozzle, which supports the qualitative explanation given above. On the other hand the data demonstrates that the RF “background” discharge is localized near to the powered electrode; further from the electrode the electron density rapidly decays. The active DC discharge exhibits some decay of the electron density downstream along the system axis as well, but just about a factor 2 in comparison with about an order of magnitude of the RF “background” discharge. That again supports the idea given above that to the formation of the plasma jet contributes the hydrodynamics of the (probably supersonic) gas flow.

There is an apparent discrepancy between the magnitude of the electron density measured in the continuous DC (Fig. 2) and pulsed DC (Fig. 3) case. Such behavior has already been observed before and reported in [4]. In that paper the optical emission spectroscopy of Ti spectral lines was performed and reported. It was found that in the continuous DC case the Ti lines intensity was approximately five times higher than in the pulsed DC case. Since the ionization energy of Ti - 6.82 eV - is much lower than that of Ar the presence of sputtered Ti atoms should contribute to substantial increase of the electron density. Further argument for higher electron density in the continuous case yields the temperature of the inside surface of the nozzle. Since the thermal conductivity of Ti is comparatively low ($0.2 \text{ Wcm}^{-1}\text{K}^{-1}$) the inner surface of the Ti nozzle may have been heated up to much higher temperature in the continuous DC case

compared to the pulsed one. Consequently, evaporation of the inner nozzle surface followed by electron impact- or photo-ionization that would further enhance the electron density cannot be excluded in the continuous DC case.

4. Conclusions

We applied the Langmuir probe diagnostic method to study the plasma parameters in the low-pressure hollow-cathode plasma jet deposition system. We measured the spatial distribution of the plasma parameters in the DC plasma jet and their temporal evolution in the pulsed DC plasma jet ignited over a background continuous RF discharge.

In the DC hollow-cathode plasma jet, the electron density decays rather slowly from the system axis to the walls of the reactor, with the position of maximum shifted from the axis. Mean electron energy is in contrary higher in the peripheral region than near the axis. The possible explanation of these effects is attributed to the geometry of the discharge and its hydrodynamic properties.

References

- [1] L. Bardos, V. Dusek, *Thin Solid Films* **158**, 265 (1988).
- [2] M. Šícha, L. Soukup, L. Jastrabík, M. Novák, M. Tichý, *Surf. Coat. Technol.* **74-75**, 212 (1995).
- [3] L. Bardos and S. Berg, *Surf. Coat. Technol.* **54/55**, 91 (1992).
- [4] P. Virostko, Z. Hubička, P. Adámek, M. Čada, J. Olejníček, M. Tichý, M. Šícha, *Contrib. Plasma Phys.* **46**, 445 (2006).
- [5] H. Barankova, L. Bardos, S. Berg, *Vacuum* **46**, 1433 (1995).
- [6] H. Barankova, L. Bardos, *Surface and Coatings Technology* **120-121**, 704 (1999).
- [7] H. Barankova, L. Bardos, L.E. Gustavsson, *Surface and Coatings Technology* **188**, 703 (2004).
- [8] L. Soukup, M. Šícha, F. Fendrych *et al.*, *Surface and Coatings Technology* **116-119**, 321 (1999).
- [9] V. Stranak, Z. Hubicka, P. Adamek *et al.*, *Surface and Coatings Technology* **201**, 2512(2006).
- [10] Z. Hubicka, M. Šícha, L. Pajasova *et al.*, *Surface and Coatings Technology* **142**, 681 (2001).
- [11] L. Bardos, S. Berg, *Surface and Coatings Technology* **54**, 91 (1992).
- [12] Z. Hubicka, M. Cada, I. Jakubec *et al.*, *Surface and Coatings Technology* **174**, 632 (2003).
- [13] N.J. Ianno, R.J. Soukup, Z. Hubicka *et al.*, *Materials, Integration and Technology for Monolithic Instruments* **869**, 133 (2005).
- [14] J. Olejnicek, Z. Hubicka, P. Virostko *et al.*, *Integrated Ferroelectrics* **81**, 227 (2006).
- [15] J. Olejnicek, Z. Hubicka, P. Virostko *et al.*, *Czechoslovak Journal of Physics* **56**, B1283 (2006).
- [16] H. Kirimura, H. Maeda, H. Murakami, T. Nakahigashi, S. Ohtani, T. Tabata, T. Hayashi, M. Kobayashi, Y. Mitsuda, N. Nakamura, H. Kuwahara, A. Doi, *Jap.J.Appl.Phys. Part 1*, **33(7B)**, 4389 (1994).
- [17] I. Langmuir, H.M. Mott-Smith, *Gen. Elec. Rev.* **26**, 731 (1923).
- [18] J.D. Swift, M.J.R. Schwar, *Electrical Probes for Plasma Diagnostics*, (Ilfie books, London, 1970).
- [19] P.M. Chung, L. Talbot and K.J. Touryan, *Electric Probes in Stationary and Flowing Plasmas: Theory and Application*, (Springer-Verlag, 1975).
- [20] M.S. Benilov, *High Temp.* **26**, 780 (1988).
- [21] V.I. Demidov, S.V. Ratynskaia, K. Rypdal, *Rev. Sci. Instr.* **73**, 3409 (2002).
- [22] S. Pfau, M. Tichý, *Langmuir probe diagnostics of low-temperature plasmas*, in *Low Temperature Plasma Physics*, 2nd Edition, R. Hippler, H. Kersten, M. Schmidt, Karl H. Schoenbach, Eds., Wiley-VCH Verlag GmbH & Co KGaA, Weinheim, 2008, ISBN 978-3-527-40673-9, pp. 175-214.
- [23] M.J. Druyvesteyn, *Z. Physik* **64**, 781 (1930).
- [24] P.A. Chatterton, J.A. Rees, W.L. Wu, K. Al-Assadi, *Vacuum* **42**, 489 (1991).
- [25] H. Sabadil, S. Klagge, M. Kammayer, *Plasma Chemistry and Plasma Processing* **8**, 425 (1988).
- [26] A. Bogaerts, A. Okhrimovskyy, N. Bager, R. Gijbels, *Plasma Sources Sci. Technol.* **14**, 191 (2005).
- [27] M. Tichý, M. Šícha, L. Bárdoš, L. Soukup, L. Jastrabík, K. Kapoun, J. Touš, Z. Mazanec, R.J. Soukup, *Contrib. Plasma Phys.* **34**, 765 (1994).